

XVII. EFFECT OF AMBIENT TEMPERATURE AND HUMIDITY ON EMISSIONS OF AN IDLING GAS TURBINE

C. W. Kauffman

University of Cincinnati
Department of Aerospace Engineering and Applied Mechanics

Environmental Protection Agency regulations pertaining to emissions standards for gas turbine engines specify the maximum quantities of the pollutant species that may be exhausted during a landing/takeoff cycle for engine inlet conditions corresponding to those of a standard day. However, only occasionally are ambient conditions those of a standard day. Correction techniques are needed therefore to relate emissions measurements actually made from an engine or combustor to those that would have occurred on a standard day.

The effects of inlet pressure, temperature, and humidity on the oxides of nitrogen produced by an engine operating at takeoff power settings were noted quite early by Lipfert (ref. 1), and subsequently numerous correction factors were formulated. These factors have been recently compiled and evaluated by Rubins and Marchionna (ref. 2). For a combustor operating at idle conditions, additional corrections were developed by Marzeski and Blazowski (ref. 3) to account for the effects of nonstandard inlet pressure and temperature on all emissions. For production samples of a given engine the effect of ambient temperature and pressure on all emissions over the complete thrust range has been correlated by Sarli, Eiler, and Marshall (ref. 4). With the exception of some limited engine test results given by Nelson, Davis, and Medlin (ref. 5), and Mosier and Roberts (ref. 6) and the work reported by Allen and Slusher (ref. 7), the effect of humidity on idle emissions apparently has received little attention although the extreme sensitivity of carbon monoxide oxidation to the presence of water vapor is well known.

To ascertain the effect of ambient relative humidity on gas turbine idle emissions, a research program was begun at the University of Cincinnati under NASA Grant NSG 3045 that encompassed both experimental and analytical work. Some of the results generated during the program are reported in this paper. Experimentally, a nonvitiating combustor rig was employed to simulate changing combustor inlet conditions as generated by changing ambient conditions. Emissions measurements were made at the combustor exit. Analytically, for carbon monoxide, a reaction kinetic scheme was applied within each zone of the combustor where initial species concentrations reflected not only local combustor characteristics but also changing ambient conditions.

EXPERIMENTAL PROGRAM

Test Apparatus

The experimental program was conducted in a closed-duct test facility, described in detail by Fear (ref. 8), located in the Engine Research Building of the NASA Lewis Research Center. A single JT8D-17 combustor can, shown in cross section in figure XVII-1, was supplied with the appropriate quantity of Jet A fuel and nonvitiating air to simulate combustor inlet conditions corresponding to specified engine inlet pressure, temperature, and humidity. The combustor installation and instrumentation are shown in figure XVII-2. The water content of the inlet air was controlled by injecting demineralized water through a spray nozzle into the hot air supplied by the preheater approximately 5 meters upstream of the combustor, thereby assuring complete vaporization. The water content of the air supplied by the preheater was continually monitored and nominally quite small (dewpoint of approximately 239 K). The combustor emissions were measured according to SAE specifications (ref. 9).

Test Conditions

The idle operating conditions, both nominal and as tested, are given in table XVII-1. In relating the ambient variables to combustor inlet variables, compressor pressure ratios of 2 to 5 were chosen along with a compressor efficiency of 80 percent. The mass flow through the combustor was calculated on the basis of a constant compressor discharge Mach number or a constant reference velocity. Since the mass flow into the combustor consists of both air and water, the combination of which may be considered as an oxidizer, the fuel flow was set to maintain a constant fuel-air ratio and not a constant fuel-oxidizer ratio. Because the combustor was of fixed geometry, three different values of the overall fuel-air ratio were used in order to affect local fuel-air ratios within the combustor.

Experimental Results

Representative values of the measured emissions from the JT8D-17 combustor are given in figures XVII-3 to XVII-6 in terms of the emission index (EI = g of pollutant/kg of fuel). All figures correspond to one simulated compressor discharge condition - a pressure ratio of 4 and a constant Mach number. On each figure, three sets of data are given - one for each overall fuel-air ratio. If all other conditions remain constant, a larger fuel-air ratio gives a higher combustor discharge temperature T_4 . Within each of the three fuel-air ratio groupings, two parameters were independently varied - the ambient temperature T_0 and the relative humidity RH. For each of the three ambient temperatures considered, data points are presented for three relative humidities, with the exception of $T_0 = 244$ K, where an extremely small quantity of water corresponds to saturation and only one value of relative humidity is given. For a fixed fuel-air ratio and zero relative humidity, an increasing ambient temperature increases the combustor discharge temperature. For a fixed fuel-air ratio and ambient temperature, increasing the relative humidity decreases the combustor discharge temperature.

In figures XVII-3 and XVII-4, the following trends are recognized: For a fixed set of ambient conditions an increase in the fuel-air ratio leads to a decrease in the hydrocarbon (HC) and carbon monoxide (CO) emission indices. For a fixed fuel-air ratio and zero humidity an increase in the ambient temperature causes a decrease in the emission indices. For a fixed fuel-air ratio and a given ambient temperature an increase in the relative humidity causes an increase in the emission indices - an effect that is especially noticeable at the highest ambient temperature, where saturation corresponds to the presence of 8.12-percent-by-mass water vapor.

Although it is difficult to accurately determine functional dependence with such limited data, some behavior is apparent. For all fuel-air ratios the slope $\left[\frac{\partial(EI_{HC})}{\partial T_4} \right]_{RH=0.0}$ is less negative than the slope $\left[\frac{\partial(EI_{HC})}{\partial T_4} \right]_{RH=1.0}$, with both becoming less negative with increasing fuel-air ratios. For all fuel-air ratios the slopes $\left[\frac{\partial(EI_{CO})}{\partial T_4} \right]_{RH=0.0}$ are nearly identical but the slope $\left[\frac{\partial(EI_{CO})}{\partial T_4} \right]_{RH=1.0}$ increases with decreasing fuel-air ratio. At the highest fuel-air ratio the two slopes are nearly identical.

The following well-known trends are evident from an examination of figure XVII-5: For a fixed set of ambient conditions an increase in the fuel-air ratio leads to an increase in the oxides of nitrogen (NO_x) emission index except at the highest absolute humidity conditions ($T_0 = 322 \text{ K}$; $RH = 100$ per cent). For a fixed fuel-air ratio and zero humidity an increase in the ambient temperature causes an increase in the emission index. For a fixed fuel-air ratio and a given ambient temperature an increase in the relative humidity causes a decrease in the emission index, again an effect that is quite noticeable when the quantities of water vapor are large. The slopes $\left[\frac{\partial(EI_{NO_x})}{\partial T_4} \right]_{RH=0.0}$ and $\left[\frac{\partial(EI_{NO_x})}{\partial T_4} \right]_{RH=1.0}$ are little affected by the value of the fuel-air ratio, and the former has a slightly smaller value than the latter.

In figure XVII-6 the nitrogen dioxide (NO_2) emission index for the lowest fuel-air ratio shows trends identical to those for the total oxides of nitrogen. It is difficult to recognize a functional dependence of the emission index on ambient conditions for the higher fuel-air ratios. Consideration of data

collected at other simulated idle operating conditions will delineate this problem further.

In this paper only a limited amount of the emissions data collected is presented, that is, those data for a compressor pressure ratio of 4 and a constant compressor discharge Mach number. A comparison of all emissions data shows that, for a given pressure ratio, little difference exists between the emissions levels and trends for the constant reference velocity and those for a constant compressor discharge Mach number. However, the increase in the pressure ratio does cause a decrease in the HC and CO emission indices and an increase in the NO_x and NO_2 emission indices. An examination of the additional data shows that the functional dependence of the NO_2 emission index is identical to that of the total NO_x emission index as long as the combustor discharge temperature is less than approximately 900 K. Above this temperature the expected quantities of NO_2 do not appear. For all data, the range in ambient conditions considered certainly produces large variations in the emission indices.

Other combustor emissions data are surprisingly similar to those collected for the JT8D-17. The emissions data of Marzeski and Blazowski (ref. 3) were collected on a T-56 combustor with two different fuels and differing primary-zone fuel-air ratios for a constant overall fuel-air ratio. The relative humidity of the inlet air was close to zero. Although the absolute values of the emission indices vary slightly for identical compressor pressure ratios, the slopes $\left[\frac{\partial(\text{EI})}{\partial T_4} \right]_{\text{RH}=0.0}$ for HC, CO, and NO_x are nearly identical. A similarity among combustors would ease the regulatory task of developing corrections for nonstandard inlet conditions.

ANALYTICAL EFFORT

Model

The experimental results indicate that the HC and CO emissions are decreased by increasing fuel-air ratio, pressure ratio, and ambient temperature, while they are increased by an increasing ambient humidity. For the

NO_x emissions the situation is just the reverse. The behavior of the NO_x emissions has been modeled to account for all effects (ref. 11). Because much of the HC emissions may result from the escape of raw fuel, it was decided to first analyze the behavior of the CO emissions. Some details of the modeling process relevant to the production of CO in the gas turbine combustor have been previously given by Morr, Heywood, and Fitch (ref. 12), and a less-detailed model but including limited ambient effects has been presented in reference 4. In attempting to define a tractable but yet accurate model of the combustion process occurring within a gas turbine combustor, conflicts will arise. In the model considered here, it is suggested that the combustor may be treated as a plug flow reactor in which there is homogeneous reaction between the perfectly mixed fuel and oxidizer under isothermal conditions corresponding to the adiabatic flame temperature. Additionally, since the kinetics representing the oxidation of a complex hydrocarbon fuel, such as Jet A, are only poorly understood, methane was chosen as the fuel to be used in the analytical effort.

The combustor inlet conditions corresponding to the temperature, pressure, and water content of the compressor discharge mass flow are identical to those in the experimental measurements. In the primary zone of the combustor the methane is instantaneously mixed with the air and water vapor mixture to obtain the desired primary-zone equivalence ratio. The mixture is then allowed to react for a period of time corresponding to an appropriate primary-zone residence time at a temperature that corresponds to the adiabatic flame temperature. The primary-zone combustion products are then instantaneously mixed again with a quantity of additional air to simulate entrance into the secondary combustion zone. The mixture is again allowed to react at a temperature representing the new adiabatic flame temperature for a period of time representing an appropriate residence time. This process is again repeated in the dilution zone.

The calculation process is begun by determining the adiabatic flame temperature for each simulated compressor discharge condition and a variety of fuel-air ratios using the NASA CEC-71 computer program (ref. 13). Each fuel-air ratio, of course, could correspond to a different location within the combustor where the local value is indeed affected by the overall fuel-air ratio. The methane-air kinetic scheme used is that given by Ay and

Sichel (ref. 14), listed in table XVII-2. The second rate constant is similar in nature to that developed by Kollrack (ref. 15). The analytical model was much more successful in reproducing the magnitude of the experimental results when this smaller value was used. It may be worthwhile to note that the species HO_2 and NO_2 are not included in the reaction scheme. The rate equation for each species is solved simultaneously by using the NASA GCKP-72 computer program (ref. 16). The initial species composition used in this program differs for each ambient condition and for each combustor region. The integration routine is carried out for a period of time corresponding to the residence time for each combustor region. Representative fuel-air ratios and residence times for the regions within the combustor are given in table XVII-3.

Analytical Results

All results presented here are for a compressor pressure ratio of 4.

Values of the adiabatic flame temperature reflecting the effects of ambient conditions are given in figure XVII-7. The well-known effect of humidity on the flame temperature is clear. At a given fuel-air ratio the effect of humidity on the equivalence ratio may also be significant, as shown in figure XVII-8.

The effect of ambient conditions on the amount of CO at the end of the primary zone is shown in a normalized fashion in figure XVII-9 for a primary-zone residence time of 1 millisecond. Here CT_{CO} is defined as the mole fraction of carbon monoxide at standard ambient conditions ($T_0 = 289$; $\text{RH} = 0$) divided by the mole fraction of carbon monoxide at non-standard ambient conditions. Three different primary-zone equivalence ratios are considered, but the effects of ambient temperature and humidity changes are the same for each. An increase in the ambient temperature causes an increase in the CO mole fraction, and an increase in the ambient humidity causes a decrease in the CO mole fraction. These effects are precisely opposite to that observed for the gas turbine but agree well with the flame results of Muller-Dethlefs and Schlader (ref. 17). These results may be simply explained by considering the effect of flame temperature

on dissociation. The species present at the end of the primary zone closely correspond to those that would be present for the case of chemical equilibrium. G. A. Miles of Detroit Diesel Allison also found the same inverse ambient effects when the primary zone was treated as a perfectly stirred reactor employing a global hydrocarbon kinetic scheme (personal communication).

In view of these results, changing ambient conditions must indeed have an effect on the kinetics in the secondary and dilution zones. The mole fraction of carbon monoxide X_{CO} exiting the combustor is given in figures XVII-10, XVII-11, and XVII-12. On each figure, one primary-zone fuel-air ratio is considered and this is diluted to lower fuel-air ratios in the secondary and dilution zones. Differing sequences are denoted by the differently shaded symbols in the figures. For each sequence, changes in both the ambient temperature and the ambient humidity are considered. The residence time for each of the three combustor regions is individually taken as 5 milliseconds.

The importance of the secondary zone on CO emissions is illustrated in figure XVII-10, where the products of combustion from a primary zone having a fuel-air ratio of 0.070 are exhausted at a dilution-zone fuel-air ratio of 0.015. The largest levels of CO emission occur for the lowest secondary-zone fuel-air ratios; that is, the CO oxidation reaction is quenched. From the results for any one of the secondary-zone fuel-air ratios, the effect of changing ambient conditions on CO emissions is evident. For zero ambient humidity an increase in the ambient temperature decreases the emissions; for a given ambient temperature an increase in the ambient humidity increases the emissions. The slopes $\left[\frac{\partial(X_{CO})}{\partial T_4} \right]_{RH=0.0}$ and $\left[\frac{\partial(X_{CO})}{\partial T_4} \right]_{RH=1.0}$ depend on the fuel-air ratio of the secondary zone.

In an actual combustor, however, each secondary zone will have a unique, corresponding dilution zone. In figure XVII-11, leaner secondary zones are paired with leaner dilution zones. Not surprisingly, the least CO is produced by the sequence with the richest secondary and dilution zones. The effect of differing ambient temperature and humidity is the same as discussed with regard to the previous figure. The slopes

$\left[\frac{\partial(X_{\text{CO}})}{\partial T_4} \right]_{\text{RH}=0.0}$ and $\left[\frac{\partial(X_{\text{CO}})}{\partial T_4} \right]_{\text{RH}=1.0}$ differ from each other and depend on the dilution sequence.

For a fixed-geometry combustor operating at constant reference velocity or constant inlet Mach number, an increase in the primary-zone fuel-air ratio will also increase the secondary and dilution fuel-air ratios. This situation is illustrated by the flow sequences in figure XVII-12. Here again the secondary and dilution zones are paired. The effect of changing ambient conditions is again obvious, but the slopes $\left[\frac{\partial(X_{\text{CO}})}{\partial T_4} \right]_{\text{RH}=0.0}$ and $\left[\frac{\partial(X_{\text{CO}})}{\partial T_4} \right]_{\text{RH}=1.0}$ are quite similar for lean and rich primary zones for the lower values of T_4 . The zero-humidity-ratio slope is only slightly more negative than the 100-percent-humidity-ratio slope for higher values of T_4 .

A comparison between the last two flow sequences in figure XVII-11 and the first two flow sequences in figure XVII-12, thereby eliminating the possibility of creating a rich dilution zone from a lean primary zone and conversely, shows that the richer primary and subsequent zones give lower CO emissions.

EXPERIMENTAL AND ANALYTICAL COMPARISONS

Both collected and calculated results show that for zero ambient relative humidity an increasing ambient temperature decreases CO emissions and that for a given ambient temperature an increasing ambient relative humidity increases CO emissions. Analytically, the latter effect could only be obtained by using the modified CO/OH rate constant. The agreement in the magnitude of the emission changes is reasonable; however, the kinetic calculations are unable to predict a sufficiently large increase in the CO emissions with increasing humidity.

Any comparison is affected by the path chosen in the kinetic model by which the primary-zone combustion products are diluted to the exit conditions. As indicated in reference 12, a Gaussian distribution should be considered for the local residence times as well as for the local fuel-air ratios.

CONCLUSIONS

Changing ambient conditions are observed and predicted to significantly affect idle emissions from a gas turbine engine. The combustor discharge temperature or adiabatic flame temperature does not uniquely determine the emissions, thereby allowing a mechanism for the normalization of emissions under differing ambient conditions. Fuel-air ratio changes that may result from engine control systems reacting to changing ambient conditions can significantly affect emissions.

REFERENCES

1. Lipfert, F. W.: Correlation of Gas Turbine Emissions Data. ASME Paper 72-GT-60, Mar. 1972.
2. Rubins, P. M.; and Marchionna, N. R.: Evaluation of NO_x Prediction Correlation Equations for Small Gas Turbines. AIAA Paper 76-612, July 1976.
3. Marzeski, J. M.; and Blazowski, W. S.: Ambient Temperature and Pressure Corrections for Aircraft Gas Turbine Idle Pollutant Emissions. ASME Paper 76-GT-130, Mar. 1976.
4. Sarli, V. J.; Eiler, D. C.; and Marshall, R. L.: Effects of Operating Variables on Gaseous Emissions. Presented at APCA Specialty Conference on Air Pollution Measurement Accuracy, New Orleans, Louisiana, Oct. 1975.
5. Nelson, A. W.; Davis, J. C.; and Medlin, C. H.: Progress in Techniques for Measurement of Gas Turbine Engine Exhaust Emissions. AIAA Paper 72-1199, Nov. 1972.
6. Mosier, S. A.; and Roberts, R.: Low Power Turbopropulsion Combustor Exhaust Emissions. PWA-FR-6487-vol. -3, Pratt & Whitney Aircraft, 1974. (AFAPL-TR-73-36-vol. -3, AD-784900.)
7. Allen, L.; and Slusher, G. R.: Ambient Temperature and Humidity Correction Factors for Exhaust Emissions from Two Classes of Aircraft Turbine Engines. FAA-RD-76-149, National Aviation Facilities Experimental Center, 1976.

8. Fear, James S.: Performance of a Small Annular Turbojet Combustor Designed for Low Cost. NASA TM X-2476, 1972.
9. Procedure for the Continuous Sampling and Measurement of Gaseous Emissions from Aircraft Gas Turbine Engines. SAE Aerospace Recommended Practice, Oct. 1, 1971.
10. Roberts, R.; Fiorentino, A. J.; and Greene, W.: Pollution Technology Program Can-Annular Combustor Engines. (PWA-5394, Pratt & Whitney Aircraft Div.; NAS 3-18548.) NASA CR-135027, 1976.
11. Blazowski, W. S.; Walsh, D. E.; and Mach, K. D.: Prediction of Aircraft Gas Turbine NO_x Emission Dependence on Engine Operating Parameters and Ambient Conditions. AIAA Paper 73-1275, Nov. 1973.
12. Morr, A. R.; Heywood, J. G.; and Fitch, A. H.: Measurements and Predictions of Carbon Monoxide Emissions from an Industrial Gas Turbine. Combust. Sci. Technol., vol. 11, nos. 3 & 4, 1975, pp. 97-109.
13. Gordon, S.; and McBride, B. J.: Computer Program for Calculation of Complex Chemical Equilibrium Compositions, Rocket Performance, Incident and Reflected Shocks; and Chapman-Jouget Detonations. NASA SP-273, 1971.
14. Ay, J. H.; and Sichel, M.: Theoretical Analysis of NO Formation Near the Primary Reaction Zone in Methane Combustion. Combust. Flame, vol. 26, no. 1, Feb. 1976, pp. 1-15.
15. Kollrack, R.: Model Calculations of the Combustion Product Distributions in the Primary Zone of a Gas Turbine Combustor. ASME Paper 76-WA/GT-7, Dec. 1976.
16. Bittker, David A.; and Scullin, Vincent D.: General Chemical Kinetics Computer Program for Static and Flow Reactions, with Application to Combustion and Shock-Tube Kinetics. NASA TN D-6586, 1972.
17. Muller-Dethlefs, K.; and Schlader, A. F.: The Effect of Steam on Flame Temperature, Burning Velocity, and Carbon Formation in Hydrocarbon Flames. Combust. Flame, vol. 27, no. 2, Oct. 1976, pp. 205-215.

IDLE JT8D-17 COMBUSTOR CONDITIONS

Nominal Operation¹⁰

Total Inlet Pressure - 2.47 atm
 Total Inlet Temperature - 393 K
 Air Flow - 1.37 kg/sec
 Fuel Flow - 0.0161 kg/sec
 Fuel/Air Ratio - 0.0117

Test Operation

Compressor Efficiency - 0.8
 Compressor Pressure Ratio - 2, 3, 4, 5
 Compressor Inlet Pressure - 1 atm
 Compressor Inlet Temperature - 244, 289, 322 K
 Compressor Inlet Relative Humidity - 0, 50, 100%
 Fuel/Air Ratio - 0.007, 0.011, 0.015
 Constant Compressor Discharge Mach Number
 $M_3 = 0.42$, or
 Constant Reference Velocity, $V_3 = 15.2$ m/sec

Table XVII-1.

KINETIC SCHEME OF METHANE-AIR COMBUSTION AND FORWARD RATE CONSTANTS

$$[k_f = AT^{\alpha} e^{-\Delta E/RT} \text{ (cm}^3/\text{mole/sec)}]$$

Reaction	A	α	ΔE
1 M + CH4 = CH3 + H	0.20E18	0.0	88332.5
2 CH4 + OH = CH3 + H2O	0.28E14	0.0	4962.5
3 CH4 + O = CH3 + OH	0.20E14	0.0	9210.4
4 CH4 + H = CH3 + H2	0.69E14	0.0	11810.8
5 CH3 + O2 = HCO + H2O	0.20E11	0.0	0.0
6 CH3 + O = HCO + H2	0.10E15	0.0	0.0
7 HCO + OH = CO + H2O	0.10E15	0.0	0.0
8 M + HCO = CO + H	0.20E13	0.5	28584.0
9 CO + OH = CO2 + H	0.56E12	0.0	600.0
	0.85E-14	7.0	-13895.0
10 H + O2 = O + OH	0.22E15	0.0	16554.9
11 O + H2 = OH + H	0.17E14	0.0	9428.8
12 O + H2O = OH + OH	0.58E14	0.0	18004.0
13 H + H2O = H2 + OH	0.84E14	0.0	20048.5
14 H + OH = H2O + M	0.40E20	-1.0	0.0
15 H + H = H2 + M	0.15E19	-1.0	0.0
16 O + O = O2 + M	0.40E18	-1.0	0.0
17 O + H = OH + M	0.53E16	0.0	5518.3
18 N + O2 = NO + O	0.64E10	1.0	6232.9
19 O + N2 = NO + N	0.14E15	0.0	75231.5
20 OH + N = NO + H	0.40E14	0.0	0.0

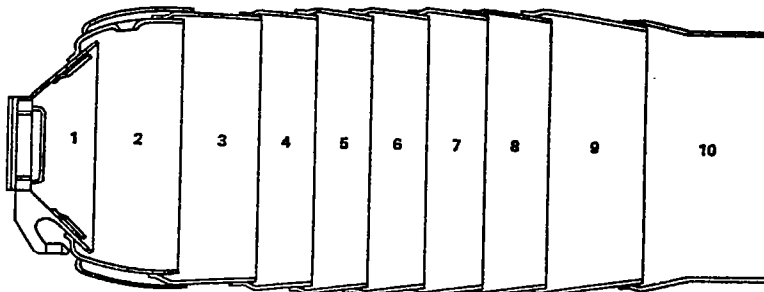
Table XVII-2.

TYPICAL LOCAL FUEL-AIR RATIOS AND AVERAGE RESIDENCE TIMES

	Primary		Secondary		Dilution	
	High	Low	High	Low	High	Low
f/a	0.071	0.048	0.034	0.019	0.012	0.011
τ (ms)	1.90	1.60	4.47	3.54	2.62	2.45

Table XVII-3.

JT8D-17 COMBUSTOR



FUEL INJECTOR AND PRIMARY SWIRLER EQUIVALENT METERING AREA 7.61%

Equivalent Metering Area

Louver Cooling Air		Combustion Air	
Panel	%	Panel	%
1	1.53	2	7.93
2	5.62	3	1.92
3	7.56	5	8.00
4	5.69	8	15.85
5	4.24	9	18.09
6	3.41		
7	3.42		
8	3.43		
9	2.78		
10	1.81		

Figure XVII-1.

COMBUSTOR ASSEMBLY AND INSTRUMENTATION SECTIONS

- △ STATIC PRESSURE
- TOTAL TEMPERATURE
- GAS SAMPLE PROBE

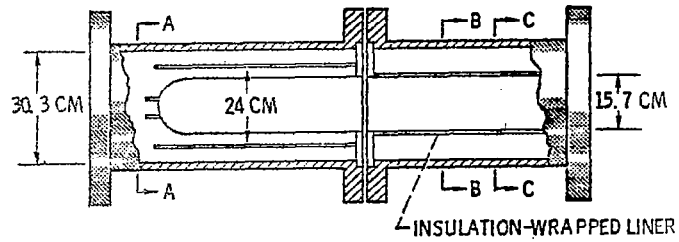
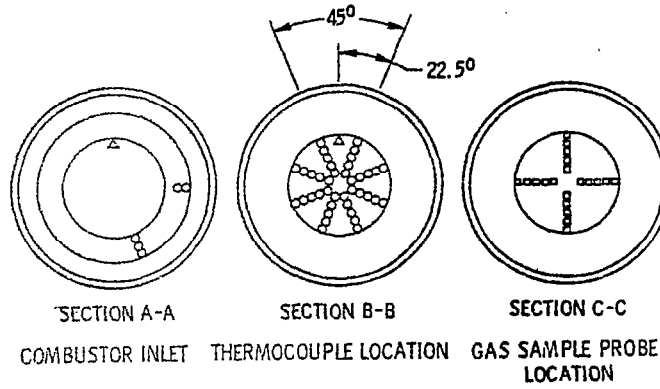


Figure XVII-2.

HYDROCARBON EMISSION INDEX, JT8D-17

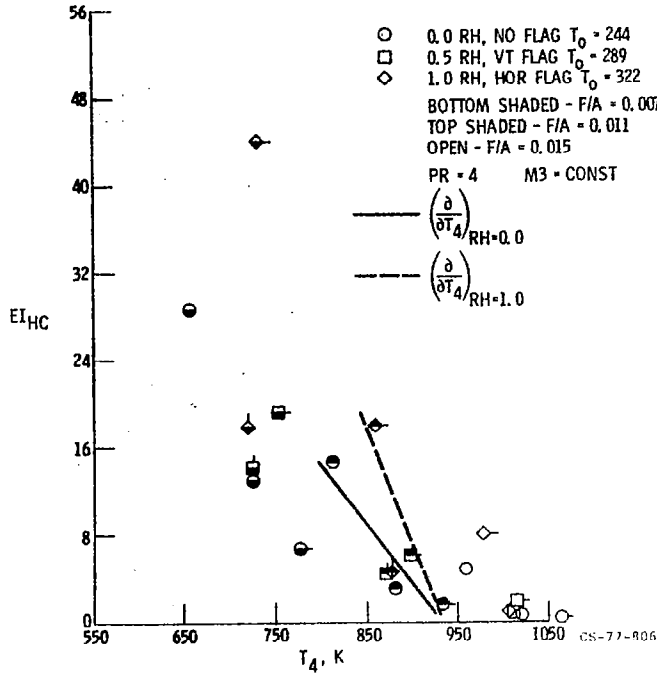


Figure XVII-3.

CARBON MONOXIDE EMISSION INDEX, JT8D-17

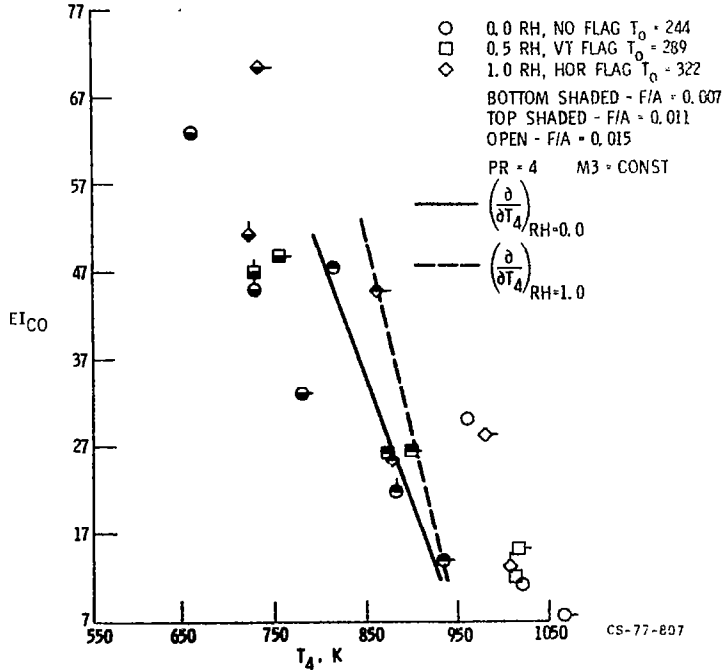
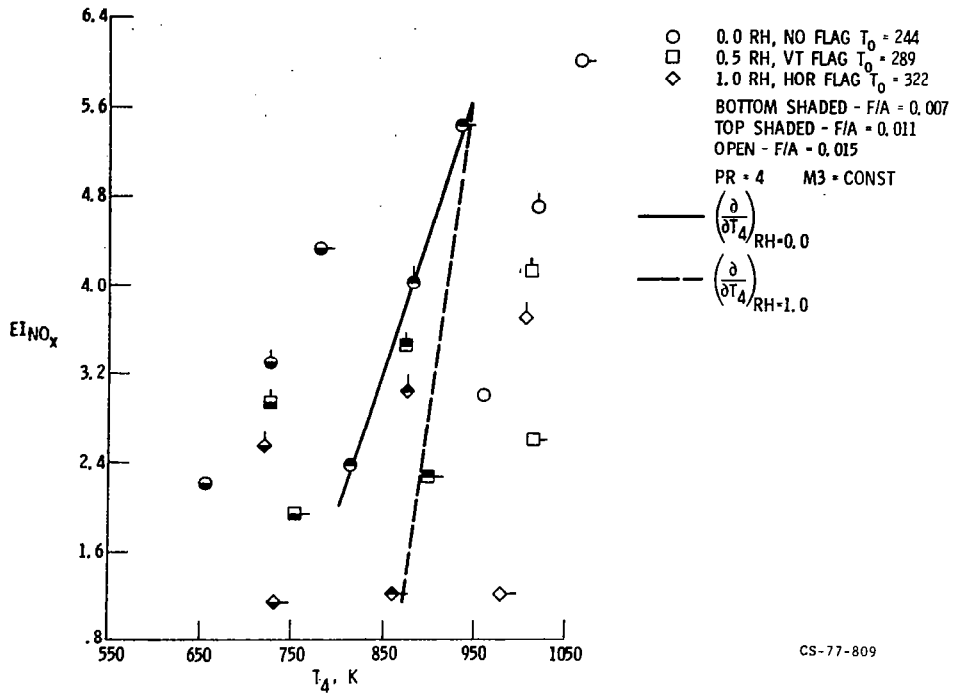


Figure XVII-4.

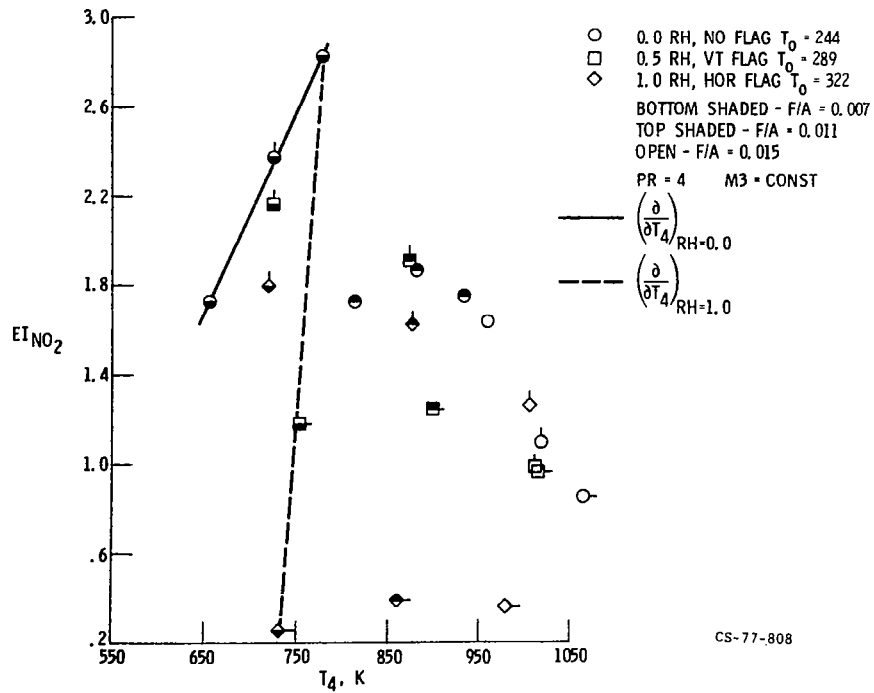
OXIDES OF NITROGEN EMISSION INDEX, JT8D-17



CS-77-809

Figure XVII-5.

NITROGEN DIOXIDE EMISSION INDEX, JT8D-17



CS-77-808

Figure XVII-6.

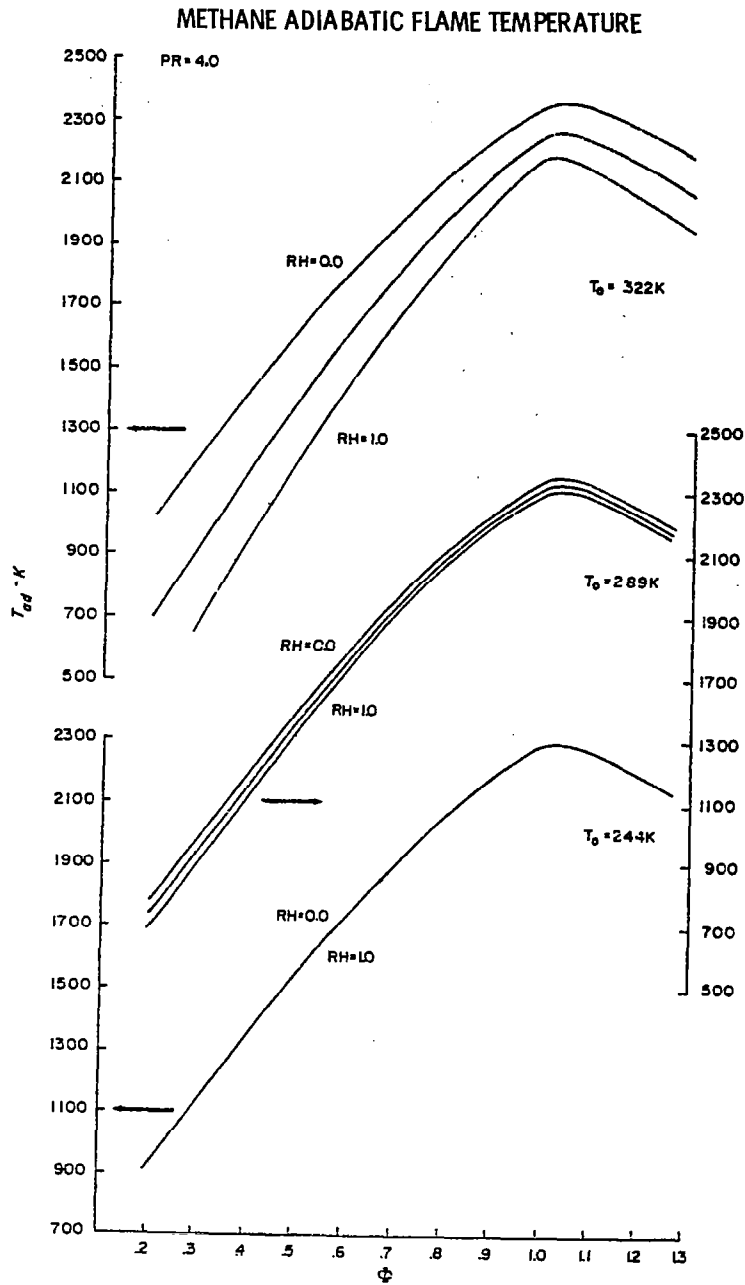


Figure XVII-7.

METHANE FUEL/AIR RATIO

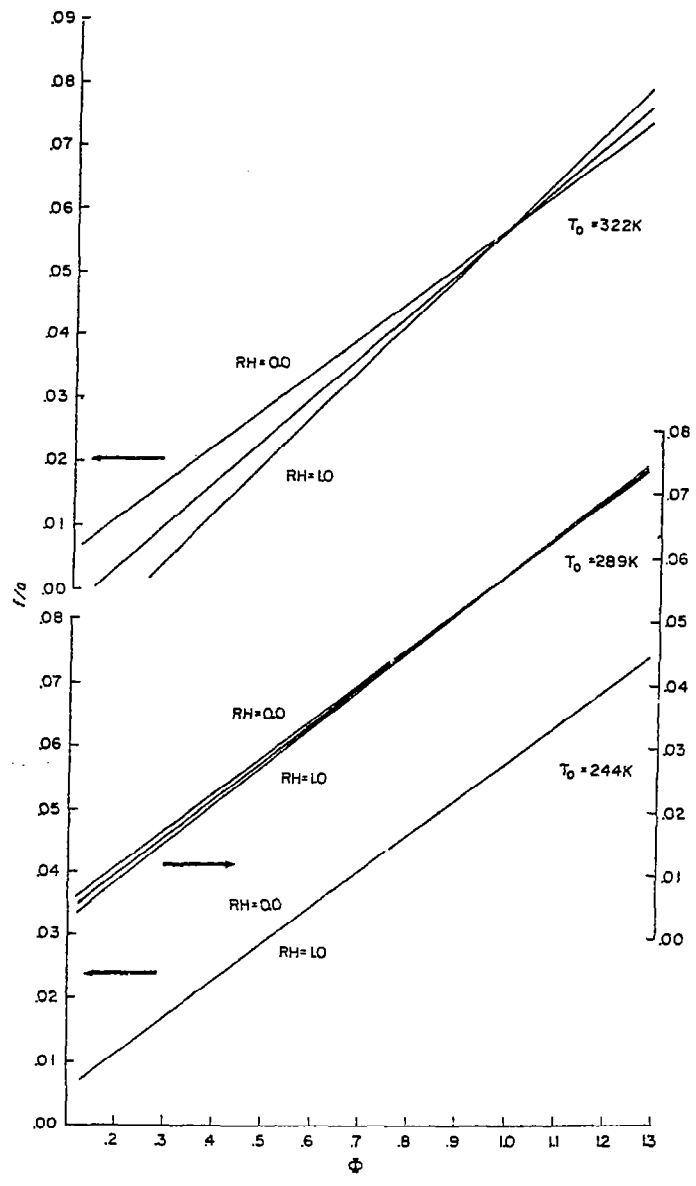


Figure XVII-8.

NORMALIZED PRIMARY ZONE CARBON MONOXIDE EMISSIONS

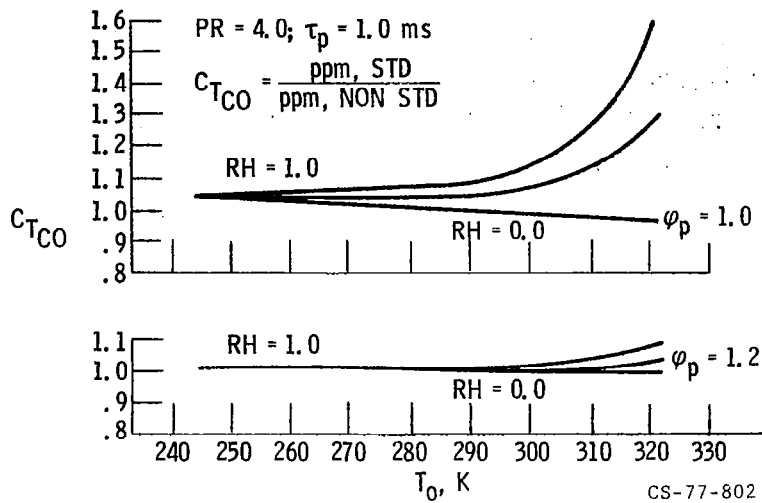


Figure XVII-9.

CARBON MONOXIDE EMISSION, METHANE KINETIC SCHEME

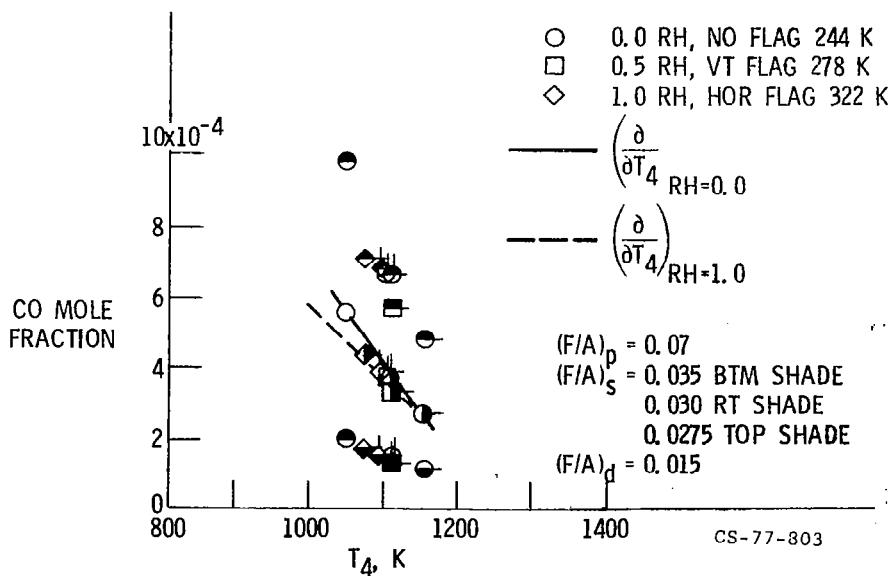


Figure XVII-10.

CARBON MONOXIDE EMISSION, METHANE KINETIC SCHEME

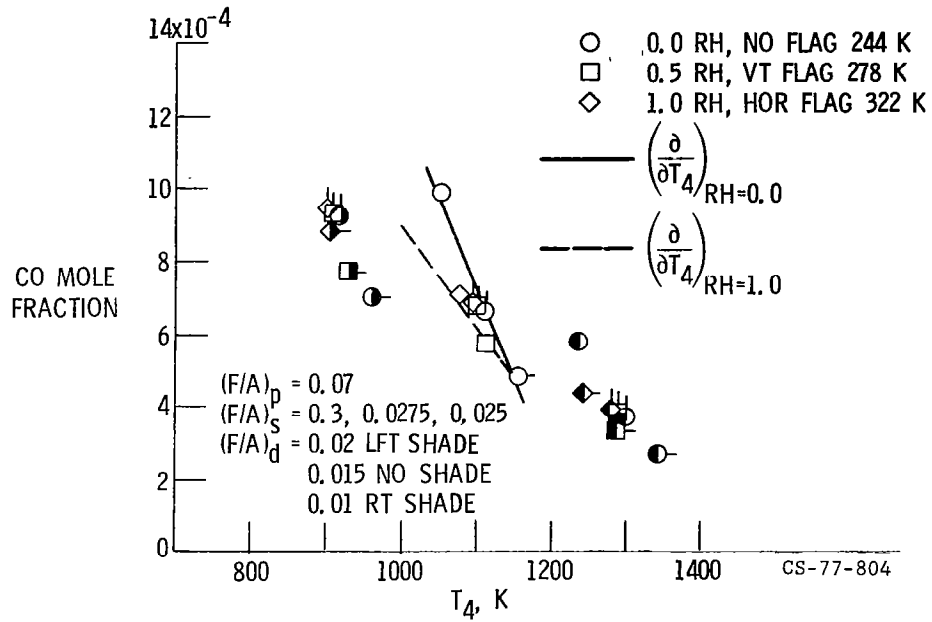


Figure XVII-11.

CARBON MONOXIDE EMISSION, METHANE KINETIC SCHEME

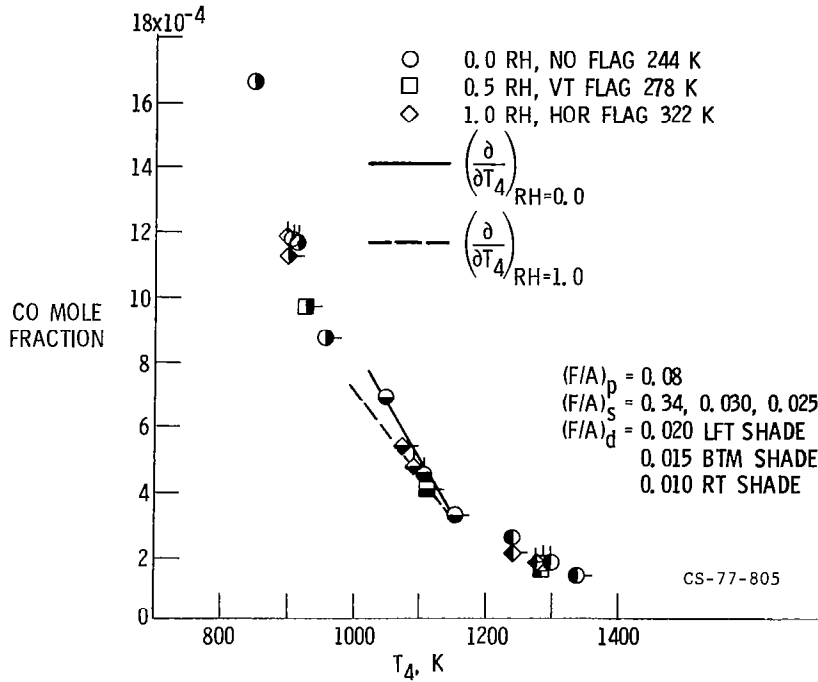


Figure XVII-12.